

Numerical study of Faraday-type nitrogen plasma magnetohydrodynamic generator

Authors: Lee, G., & Kim, H.R*.

Journal Information:

- **Journal:** Journal of the Korean Physical Society
 - **Year:** 2021
 - **Volume:** 78(7)
 - **Pages:** 600-606
 - **DOI:** <https://doi.org/10.1007/s40042-021-00116-z>
-

ACCEPTED MANUSCRIPT NOTICE

© 2021. This is a post-peer-review, pre-copyedit version of an article published in *Journal of the Korean Physical Society*.

Disclaimer: This is a post-peer-review, pre-copyedit version of an article published in *Journal of the Korean Physical Society*. The final authenticated version is available online at: <https://doi.org/10.1007/s40042-021-00116-z>

Please cite the published version.

Numerical study of Faraday-type nitrogen plasma magnetohydrodynamic generator

Geun Hyeong Lee, Hee Reyoung Kim*

*Ulsan National Institute of Science and Technology, Department of Nuclear Engineering,
Ulsan 689-798, Republic of Korea
kimhr@unist.ac.kr*

Short title: Variable analysis of Faraday-type Nitrogen Plasma MHD Generator

Abstract

The variables of a magnetohydrodynamic (MHD) generator were analyzed for the application of a cogeneration system in a coal-fired power station. The MHD generator system is more efficient than other generation systems, owing to its high working temperature. The system is typically combined with a steam generator because high-temperature conditions result in significant residual heat. The magnetic and electric fields, which directly affect the electric output, should be analyzed under this condition. The electric field, velocity, and magnetic flux density of the MHD generator were analyzed, and nitrogen plasma in the temperature range of 3000 K was employed. The electric power was affected by velocity, magnetic flux density, and electric conductivity. The electric power was proportional to the square of the velocity and magnetic flux density and proportional to the electrical conductivity. A de Laval nozzle was adopted to increase the velocity. The electric power was optimized according to the angle of the de Laval nozzle. Power generation was derived through the geometrical size and magnetic flux density of the prototype Faraday-type nitrogen plasma MHD generator.

Keywords: Magnetohydrodynamic generator; de Laval nozzle; Velocity; Magnetic flux density; Power

Nomenclatures

\vec{B}	Magnetic flux density [T]
\vec{B}_0	External supplied magnetic flux density [T]
\vec{b}	Induced magnetic flux density [T]
\vec{E}	Electric field intensity [V/m]
\vec{J}	Current density [A/m ²]
L	Characteristic length scale [m]
P	Power density [W/m ³]
\vec{p}	Developed pressure [Pa]
t	Time [s]
\vec{U}	Fluid velocity [m/s]
μ	Magnetic permeability [H/m]
μ_d	Dynamic viscosity [Pa·s]
ν	Kinematic viscosity [m ² /s]
ρ	Density [kg/m ³]
σ	Electrical conductivity [1/(Ω · m)]

1. Introduction

Magnetohydrodynamic (MHD) generation is a method developed using Ohm's law that utilizes an external magnetic field where the velocity of a fluid exists. The MHD generator is more efficient than other generator technologies and can be applied to coal-fired power stations [1].

Nitrogen is the main component in the emitted off-gas in coal-fired power stations. The nitrogen gas is adopted as a fluid to check the generation tendency of the off-gas. The plasma state of the exhaust gas is used as a fluid in the generator, and the electrically conductive plasma

electromagnetically reacts with the external magnetic flux. Consequently, electricity is generated by the MHD generator. MHD generation systems are primarily divided into two types: closed- and open-cycle generation systems. The closed-cycle generation system uses noble gases as the working fluid, and a heat exchanger attached to a heat source is used to heat the gas. Closed-cycle systems have the advantage of higher electrical conductivity over open-cycle systems as noble gases more readily transition to the plasma state compared to other gases [2,3]. Consequently, they have higher efficiency than open-cycle generation systems at 55% and 46% respectively [4]. However, a closed system has relative difficulty raising the temperature because it is not directly heating the gas. The open-cycle generation system has the advantage of raising the temperature easily, and is additionally environmentally friendly as the process removes the oxides from nitrogen oxide, sulfur oxide, and carbon dioxide found in the working fluid when the temperature is approximately 3000 K [5,6]. An open-cycle generation system raises the temperature more easily because it directly uses the exhaust gas from the boiler. The carbon is combusted at approximately 1400 °C, and the phase change of the exhaust gas occurs at temperatures above 2000 °C. Therefore, to achieve electrically conductive plasma, a thermal storage system is required. In the cogeneration system, fluid gas is created in the boiler and is transported to the thermal storage system. After generation, the residual heat raises the temperature of the air in the air preheater system, and the steam generator produces electricity using the heated air. Finally, a Faraday-type generator is typically more efficient in a linear-shape MHD generator than in a Hall-type generator [7]. Thus, all things considered, we analyze the electromagnetic variables of a Faraday-type MHD generator using an open-cycle system. The resultant power was determined to be 12900 W based on the geometrical size and in relation to precedent studies where powers of 10600 W and 11500 W were produced in prototypes [8,9]. In this study, the power characteristic of the MHD generator as it relates to the geometrical variable and magnetic flux density was

investigated. In addition, a sketch design for a nitrogen plasma de Laval nozzle is presented, and power analysis carried out.

2. Methods

The MHD generator is divided into three parts; the magnet, flow channel, and electrode. The exhausted gas, which is in the plasma state, passes through the flow channel while receiving a magnetic flux from a permanent magnet. The interaction between the velocity of the fluid and the magnetic flux generates electricity. The basic equation of MHD generator system is the magnetohydrodynamic equations expressed in Eq. (1)

$$\frac{\partial \vec{U}}{\partial t} + (\vec{U} \cdot \nabla) \vec{U} = -\frac{1}{\rho} \nabla p + \nu \nabla^2 \vec{U} + \frac{1}{\rho} \vec{J} \times \vec{B}. \quad (1)$$

The magnetic flux density, electrical conductivity, and velocity were analyzed using the COMSOL Multiphysics 5.5 code simulation system [10,11,12]. The finite element method was used to calculate the trend of the MHD generator. The equation used for the code simulation is the electromagnetic induction method, which is provided in Eq. (2)

$$\frac{\partial \vec{B}}{\partial t} + (\vec{U} \cdot \nabla) \vec{B} = \frac{1}{\mu\sigma} \nabla^2 \vec{B} + (\vec{B} \cdot \nabla) \vec{U}. \quad (2)$$

The magnetic fields can be divided into two types: an externally supplied magnetic field (B_0) and an induced magnetic field (b) owing to fluid movement. From Maxwell's equations, the externally supplied magnetic field can be expressed as follows:

$$\nabla^2 \vec{B}_0 - \mu\sigma \frac{\partial \vec{B}_0}{\partial t} = 0. \quad (3)$$

The input pressure, input velocity, and output pressure were utilized as boundary values in the simulation. As boundary conditions, the velocity at the wall, the current density in the normal direction at the end of the analytical area, and the magnetic flux density in the tangential direction at the end of the analytical area are as follows [13]:

$$U_{wall} = 0, \quad (4)$$

$$J_{normal} = 0, \quad (5)$$

$$B_{tangential} = 0. \quad (6)$$

The power density is calculated by multiplying the obtained electric field and electrical conductivity as follows:

$$P = \sigma(\vec{E} + \vec{U} \times \vec{B})^2. \quad (7)$$

It is difficult to raise the magnetic flux density past a certain level to increase the output, so we considered increasing the input velocity. As a result, we adopted a de Laval nozzle, shown in Figure 1(b), which can dramatically increase the input velocity, enabling a high output Faraday-type generator. In the case of linear MHD generator, shown in Figure 1(a), the boundary conditions are inlet velocity, and outlet pressure with fully developed flow. The boundary conditions used with the de Laval nozzle, shown in Figure 1(b), are a pressure inlet of 100 bar, velocity inlet of 10 m/s, and outlet pressure of 1 bar.

3. Results and discussion

3.1. General characteristics

The variable characteristic of the Faraday-type MHD generator was analyzed using the COMSOL 5.5 code simulator. First, we investigated the characteristics of the variables using linear MHD generator analysis, and we then determined the geometrical size and variables of the generator using a de Laval nozzle [14,15]. A schematic of the linear generator is represented in Figure 1(a). The magnet generates a magnetic field in the flow channel, and the electric field is created by the interaction of the velocity and magnetic field. The velocity profile, which is dependent on the inlet velocity, was parabolic, as shown in Figure 2. The shape of the velocity profile remained constant as the inlet velocity increased when measured at a magnetic flux density of 5 T and electrical conductivity of 30 S/m, and there is no effect on the shape of the velocity profile because the increases in the electromagnetic force and viscous force owing to

the flow velocity are the same. Figure 3 shows the intensity of the electric field dependent on the inlet velocity, which follows the trend of the velocity profile. This occurs because the more the speed is increased, the more the current is induced, owing to Ohm's law. However, electric fields induced by the velocity and magnetic fields did not exhibit a zero value, owing to the presence of an electric current. This affects the power density characteristics. Figure 4 shows the velocity profile dependent on the electric conductivity. The larger the electrical conductivity, the larger the Lorentz force induced in the opposite direction of the flow velocity, which results in slower speeds at the center of the fluid, resulting in a Hartmann number of 167, which represents the ratio between the electromagnetic force and viscous force ($= BL \sqrt{\frac{\sigma}{\mu_d}}$).

Figure 5 shows the distribution of the electric fields according to the electrical conductivity, which is similar to the propensity of the velocity. At an electrical conductivity of 1000 S/m, the velocity at the middle position decreased, which resulted in 60% of the values of the electric fields in the middle section. The Hartmann number increases as the electrical conductivity increases. This indicates that the Lorentz force that is applied in the reverse direction to fluid velocity increases as the fluid moves, thereby decreasing the electric field in the central part [16]. The electric field profile is dependent on the magnetic flux density, and was simulated under the conditions of a conductivity of 30 S/m and velocity of 10 m/s; this is shown in Figure 6. The electric field increased linearly as the magnetic flux density increased. As the magnetic flux density increases, only the Hartmann number increases; however, at a magnetic flux density of 5 T, the Hartmann number is 29, and the electromagnetic force, which is in the opposite direction to the fluid, is not dominant. No reduction in the central electric field was observed below values of 30 S/m, owing to the low electromagnetic force.

The power density graphs dependent on the magnetic flux density, inlet velocity, and electrical conductivity are shown in Figures 7–9. The magnetic flux density and electrical

conductivity, which are fixed for interpretation, are 5 T and 30 S/m, respectively. The magnetic field was set to 5 T to obtain the highest power density. The electrical conductivity was set to 30 S/m, and this can be achieved when the plasma seed material has a mass fraction of 1% [2]. The power density along the magnetic field tended to be proportional to the square of the magnetic flux density, as shown in Figure 7, as the strength of the electric field is directly proportional to it. In the case of Figure 8, the power density was proportional to the square of the velocity. Furthermore, in Figure 9, the power density was proportional to the electrical conductivity because it only affected the shape of the velocity distribution. The velocity and magnetic flux density were the dominant values. The de Laval nozzle was adopted to produce a high velocity condition (> 1 Mach) [17].

3.2. Power estimation

A schematic of the de Laval nozzle MHD generator is presented in Figure 1 (b). The electric field is generated using the vector product of the fluid velocity and magnetic flux density from the permanent magnet ($\text{Sm}_2\text{Co}_{17}$). The mesh structure, which is used for analysis, is presented in Figure 10. As a result of utilizing the corresponding mesh shape, the error according to the iteration number was simulated to be 10^{-5} . Figure 11 shows the change in the generated power according to the angle of the nozzle. As the angle increased, the area in which the current is generated increased, which increased the power. However, there was a limit to the transmitted strength of the magnet; thus, the total power was reduced at an angle of 12° or higher. The optimal angle was 12° . The magnetic flux density distribution is shown in Figure 12. A samarium cobalt magnet was adopted, owing to its high permissible temperature. The height of the magnet was 50 mm, considering the feasibility of production. The mean magnetic flux density in the nozzle was 0.17 T. The velocity distribution is shown in Figure 13. A high-pressure fluid enters the nozzle, and the fluid is accelerated through the nozzle, which has a smaller internal cross-sectional area. The fluid is reaccelerated through the higher cross-

sectional area of the nozzle, owing to supersonic speed; this results in a maximum velocity of 3500 m/s. Figure 14 shows the power density distribution of the generator. The power is related to the square of the speed and magnetic flux density, exhibiting a maximum power density of 1.8×10^7 W/m³ at the front of the nozzle with a strong magnetic flux density. The total generated power as follows from the power density was 12900 W with an optimum angle of 12° and height of 50 mm.

Our results are discussed in comparison with those of Huang's study [9]. In Huang's study, the Faraday-type linear MHD generator was analyzed with an average velocity of 3400 m/s and conductivity of 10 S/m to derive the power according to the magnetic field. In the study, 5042 W of power was generated based on 1 T of magnetic flux density. The simulation used in the current study was applied to the results of Huang's study. The strength of the magnet was increased to meet the conditions of an average magnetic flux density of 1 T; the conditions of the velocity and electrical conductivity were met. When the corresponding results were applied, a power of 5220 W was derived, which has a difference of 3.5% from that of Huang's study. These differences exist because Huang's study uses the linear form of generator, whereas the current study uses the de Laval nozzle form. This results in different structural positions for the magnets; thus, the uniformity of the magnetic flux density is different, as shown in Figure 15. The power tends to be proportional to the square of the magnetic flux density, as shown in Figure 16. Thus, under the same mean magnetic flux density conditions, the form of the uneven magnetic field produced a slightly higher power, which created a difference in the resulting values.

4. Conclusions

We analyzed the change in the electromagnetic variables in a Faraday-type nitrogen plasma MHD generator and the changes in power owing to these variables. The power density was

verified via simulations. The results exhibited a proportional relationship between the square of the magnetic flux density and velocity and a proportional relationship with the electrical conductivity. The de Laval nozzle enabled a velocity of 3500 m/s, which can efficiently increase the generated power. We determined that the optimized power of the electrically conducting nitrogen plasma MHD generator, taking into account its geometrical size, was 12900 W, which had the specific power density characteristics of the magnetohydrodynamic variables in the permanent magnet environment.

Acknowledgement

This research was supported by the Korea Electric Power Corporation (**R18XA06-26**) and the Rare Isotope Science Project of the Institute for Basic Science funded by Ministry of Science and ICT and NRF of Republic of Korea (**2013M7A1A1075764**).

Reference

- [1] S. Anghiae and A. Ferrari, In *Proceedings of the 30th International Electric Propulsion Conference* (Florence, Italy, September 17–20, 2007).
- [2] V. D. Dhareppagol and A. Saurav, *Int. J. Adv. Electl. Electrn. Engg.* **2**, 2278 (2013).
- [3] T. Fujino, T. Murakami, Y. Okuno and H. Yamasaki, *IEEE T. Plasma Sci.* **31**, 166 (2003).
- [4] Y. Inui, S. Yanagisawa and T. Ishida, *Energy conversion and management*. **44**, 597 (2003)
- [5] V. R. Malghan, *Energy Convers. Manag.* **37**, 569 (1996).
- [6] M. Ishikawa, M. Steinberg, *Energy conversion and management*. **39**, 529 (1998)
- [7] V.S. Slavin and K.A. Finniov, *12th Int. Conf. MHD Power Generation High Temperature Technol.* **2**, 539 (1999).
- [8] T.M. York and H. Tang, *Introduction to plasmas and plasma dynamics: with reviews of application in space propulsion, magnetic fusion and space physics* (Elsevier Inc, 2015).
- [9] P. Lu, R. Fang and H. Huang, *Acs OMEGA*. **5**, 31164 (2020).
- [10] COMSOL: Multiphysics Software for Optimizing Designs, <https://www.comsol.com/>, Accessed 25 Jan 2020.
- [11] L. P. Harris, *J. Appl. Phys.* **34**, 2958 (1963).
- [12] M. Petrick, B. I. Shumiatskiĭ and B. I. Shumiatskiĭ, *Open-cycle magnetohydrodynamic electrical power generation* (Argonne National Laboratory, 1978).
- [13] T. Sakai, M. Matsumoto, T. Murakami and Y. Okuno, *Electrical Engineering in Japan* **179**, 23 (2012).
- [14] R. R. Kumar and Y. Devarajan, *Int. J. Ambient Energy*, 1 (2018).
- [15] E. Davis, C. Woodside, H. Kim, E. D. Huckaby, M. Bowen, L. Aspitarte, P. Thomsen and D. B. Oryshchyn, *Temperature and Heat Flux Measurements in a Direct Fired Laboratory Magnetohydrodynamic Generator Channel*. National Energy Technology Laboratory (NETL),

Pittsburgh, PA, Morgantown, WV (United States), 2020. Available online at:
<https://www.osti.gov/servlets/purl/1642204> (Accessed:).

[16] H. Yamaguchi, X. D. Niu and X. R. Zhang, Int. J. Energy Res. 35, 209 (2011).

[17] RAMESH KUMAR, R.; DEVARAJAN, Yuvarajan. CFD simulation analysis of two-dimensional convergent-divergent nozzle. *International Journal of Ambient Energy*, 2020, 41.13: 1505-1515.

Figure captions

- Figure 1 Schematic of (a) linear MHD generator (b) de Laval MHD generator
- Figure 2 Velocity profiles (a) 1D dependent on inlet velocity (b) 2D in a square channel
at velocity condition of 100 m/s
- Figure 3 Electric field profiles dependent on inlet velocity
- Figure 4 Velocity profiles dependent on electrical conductivity
- Figure 5 Electric field profiles dependent on electrical conductivity
- Figure 6 Electric field profiles dependent on magnetic flux density
- Figure 7 Power density dependent on magnetic flux density
- Figure 8 Power density dependent on inlet velocity
- Figure 9 Power density dependent on electrical conductivity
- Figure 10 Mesh condition of a de Laval MHD generator
- Figure 11 Generated power dependent on the de Laval nozzle angle
- Figure 12 Magnetic flux density distribution of a de Laval nozzle MHD generator
- Figure 13 Velocity distribution of a de Laval nozzle MHD generator
- Figure 14 Power density distribution of a de Laval nozzle MHD generator
- Figure 15 Magnetic flux density distribution of an MHD generator with data from Huang
- Figure 16 Power density distribution of MHD generator with data from Huang

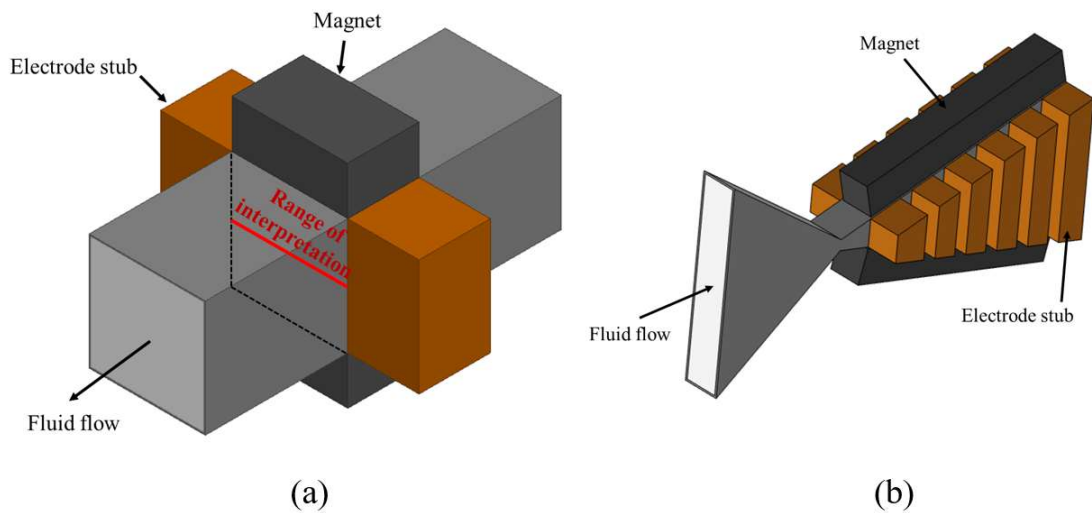


Figure 1

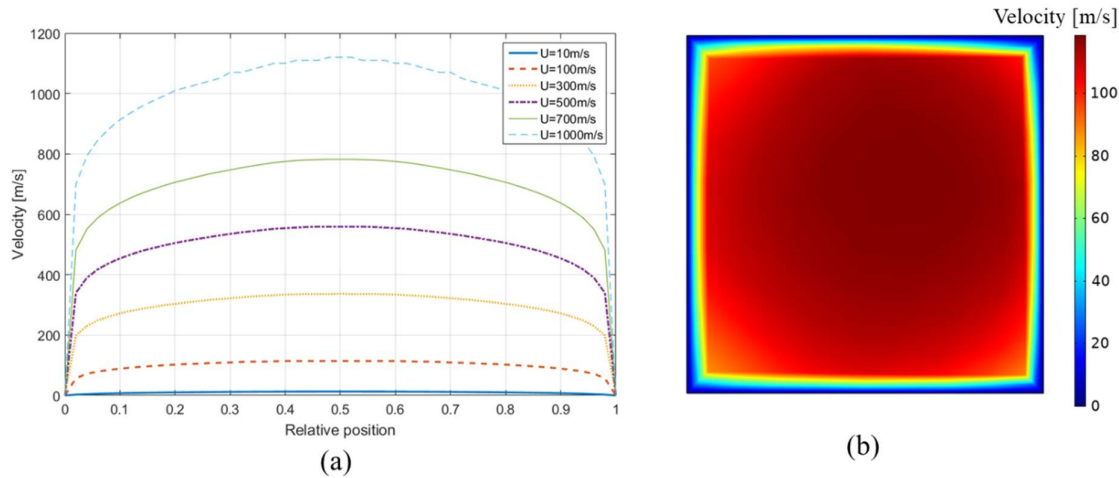


Figure 2

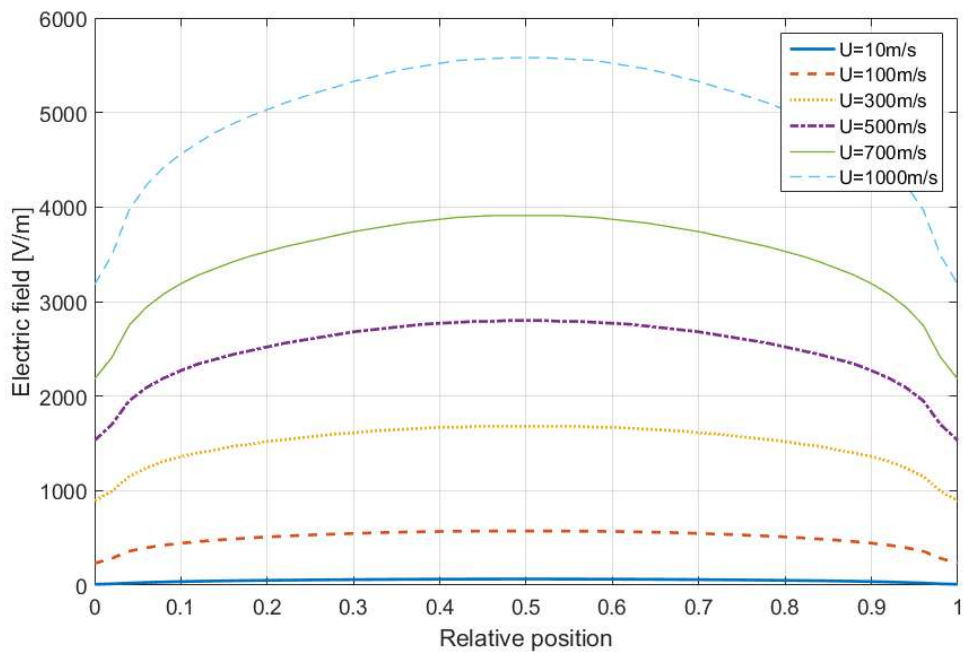


Figure 3

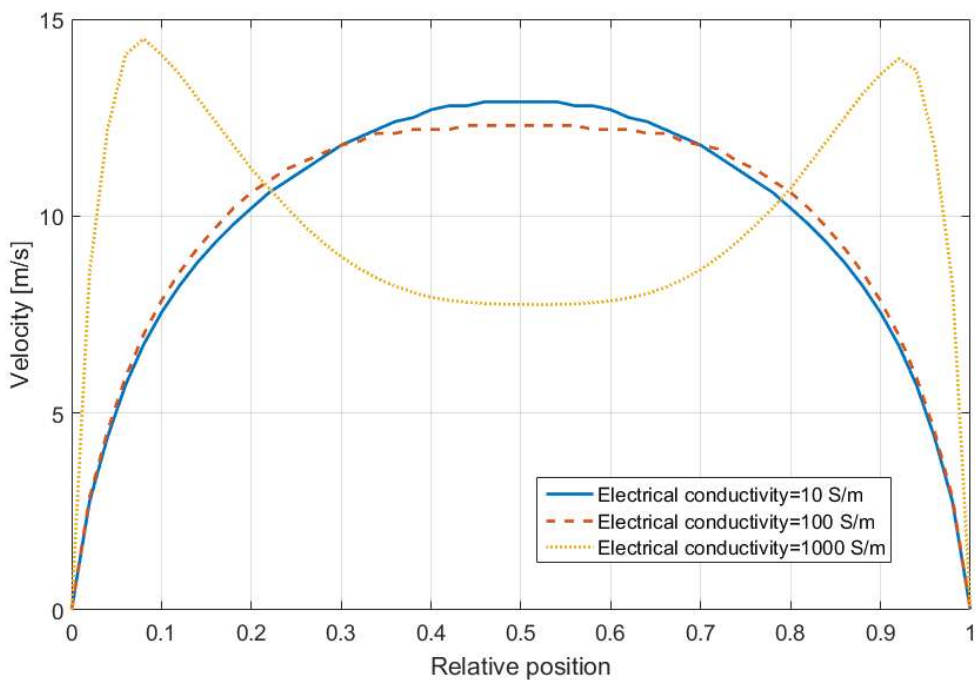


Figure 4

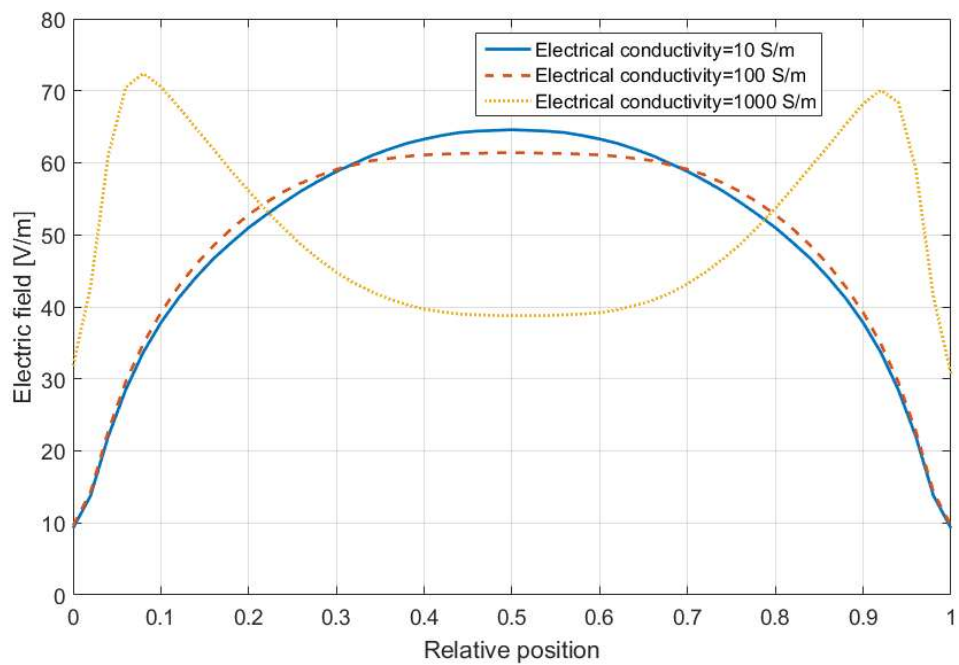


Figure 5

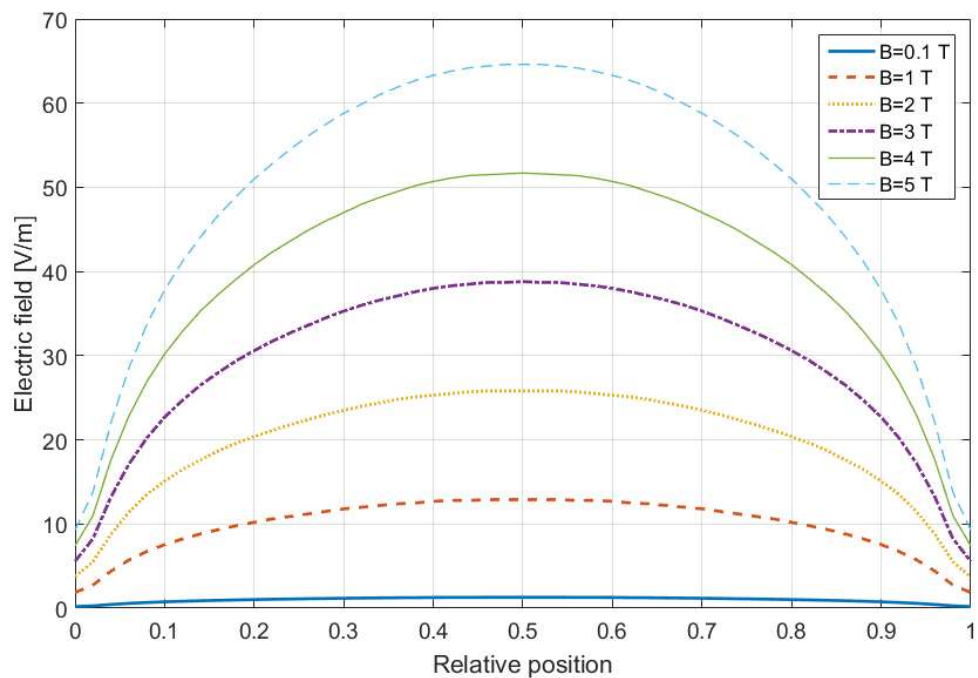


Figure 6

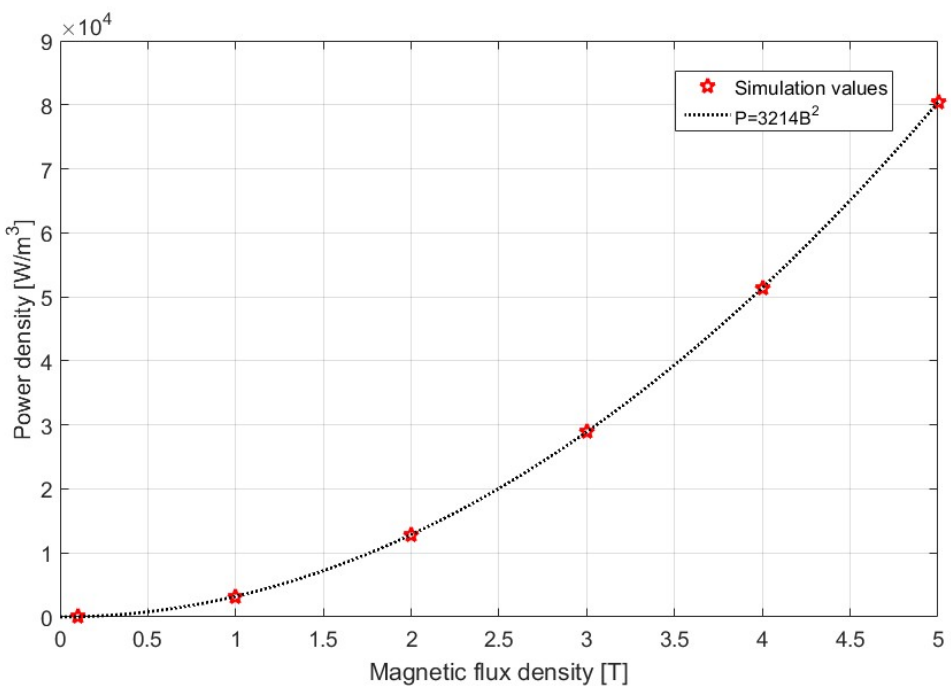


Figure 7

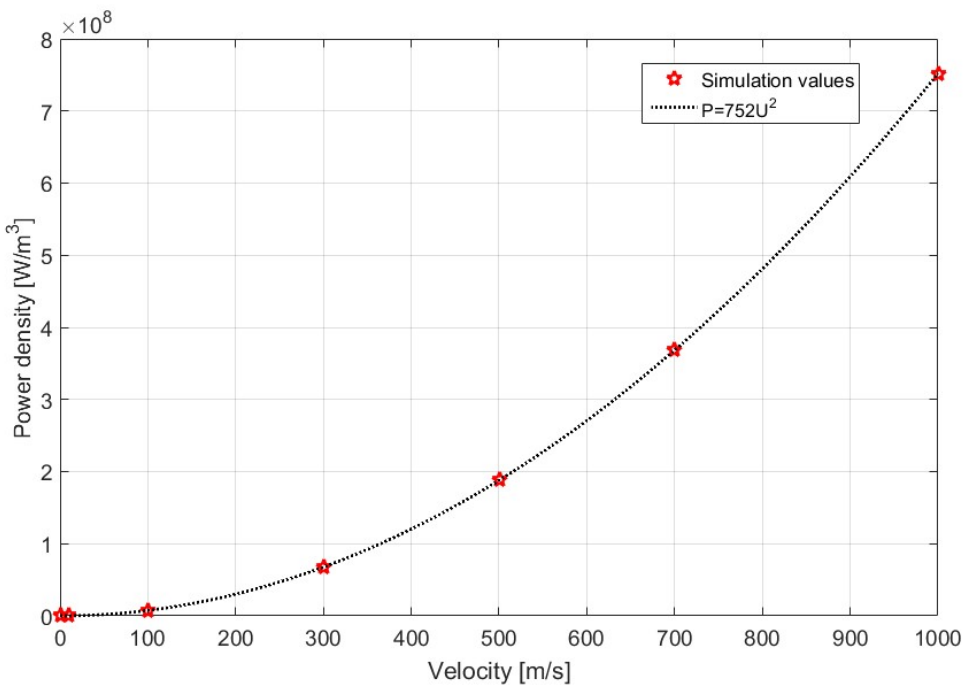


Figure 8

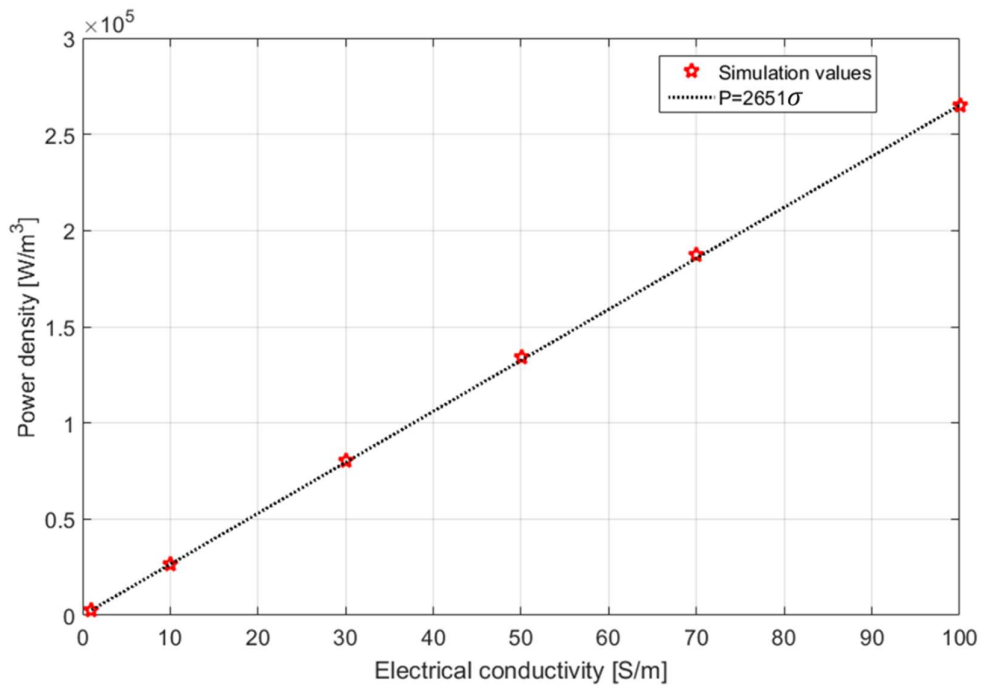


Figure 9

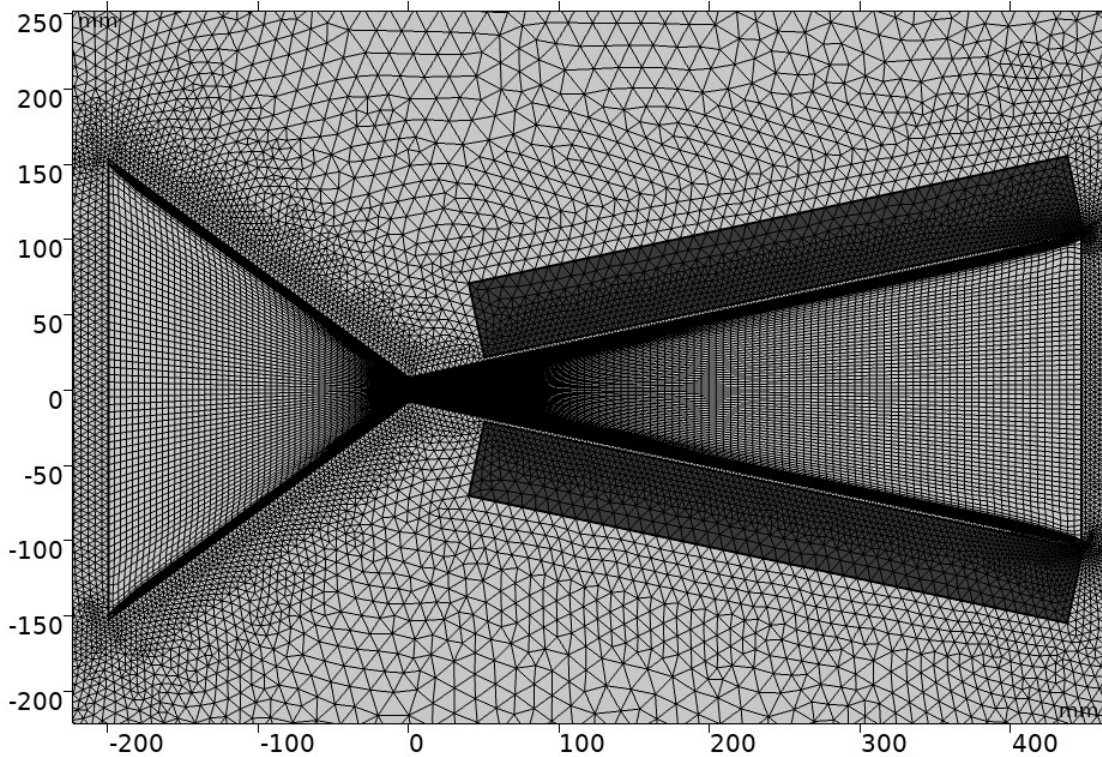


Figure 10

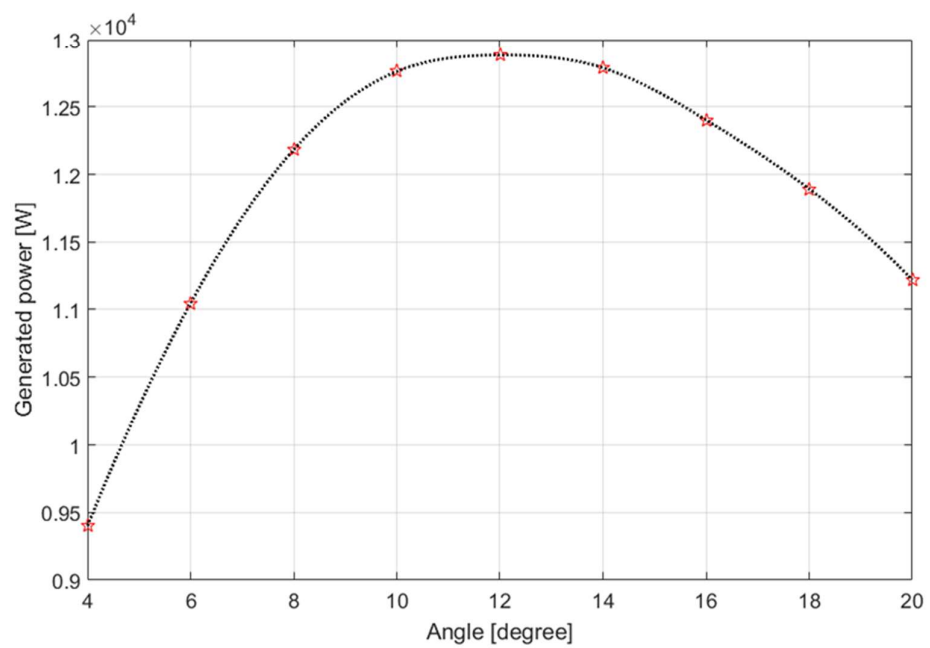
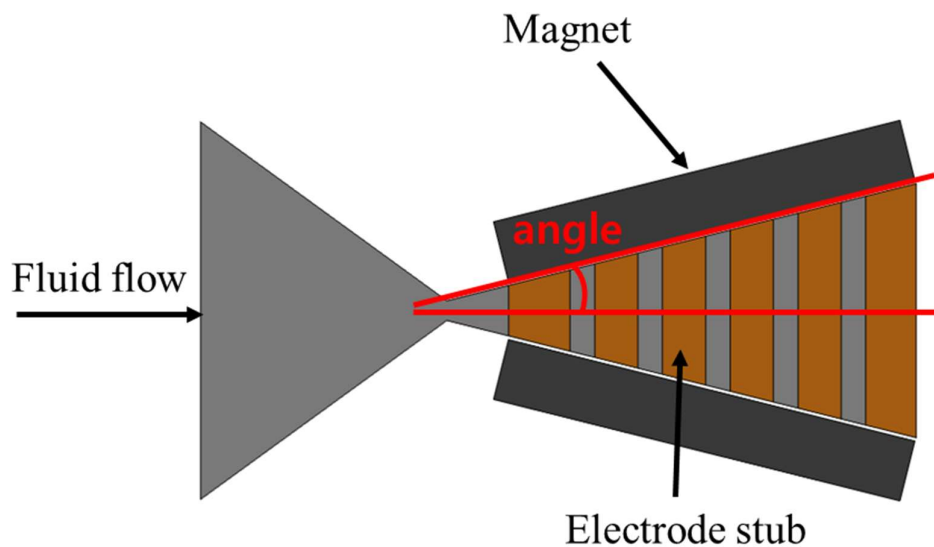


Figure 11

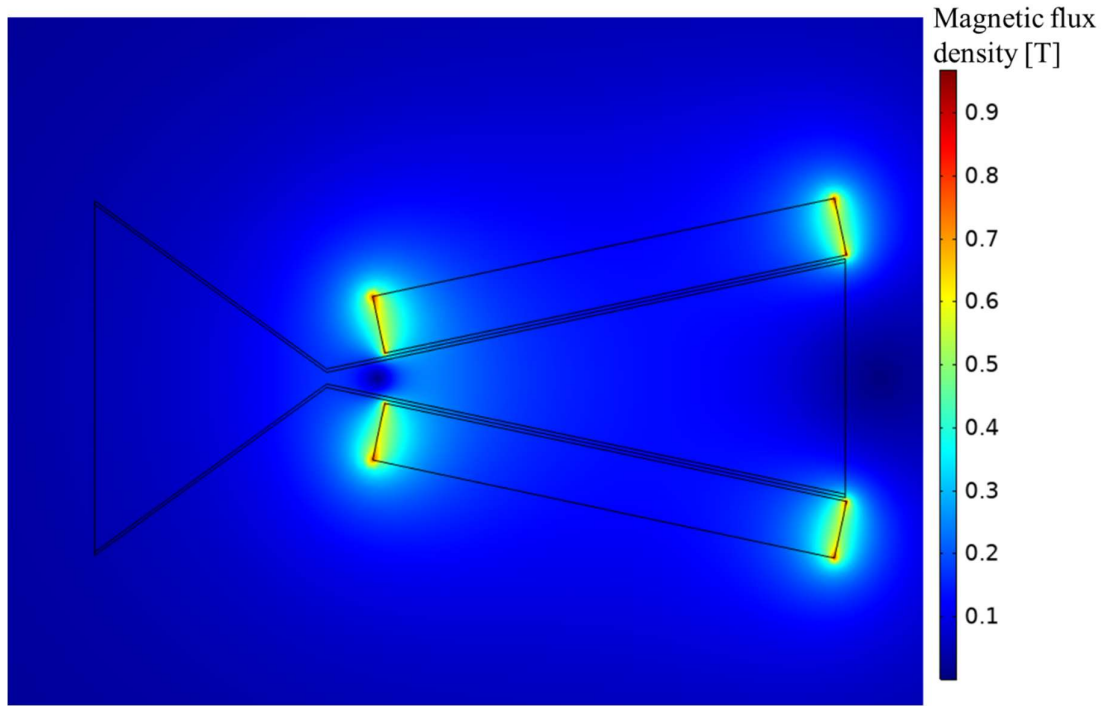


Figure 12

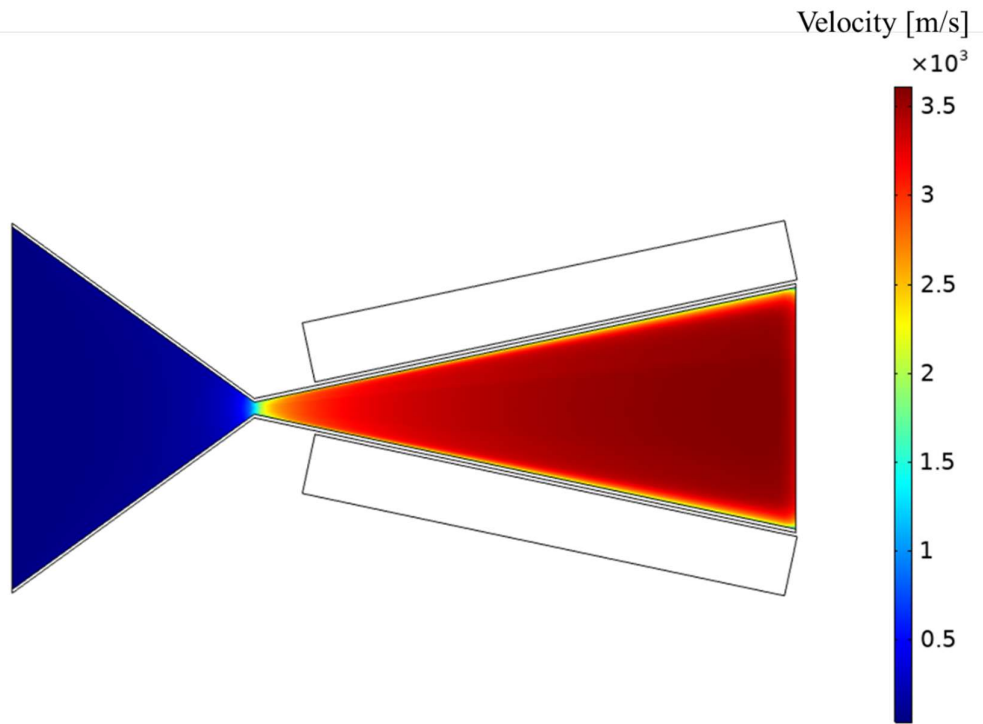


Figure 13

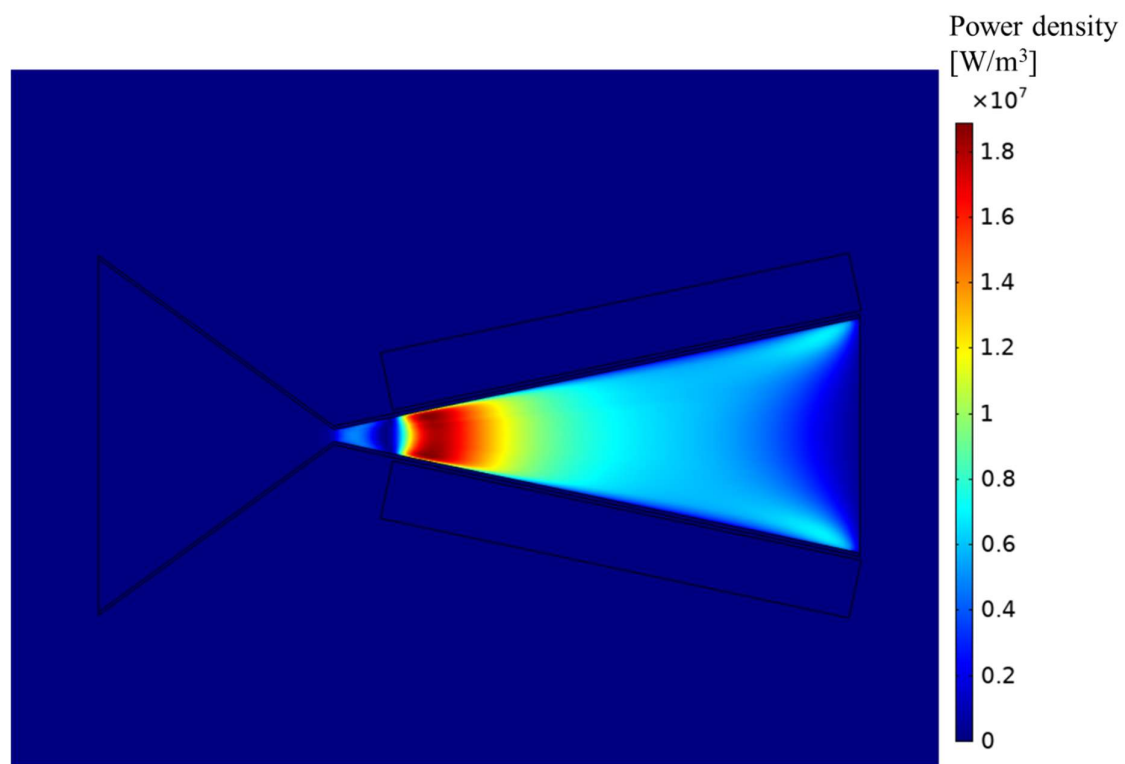


Figure 14

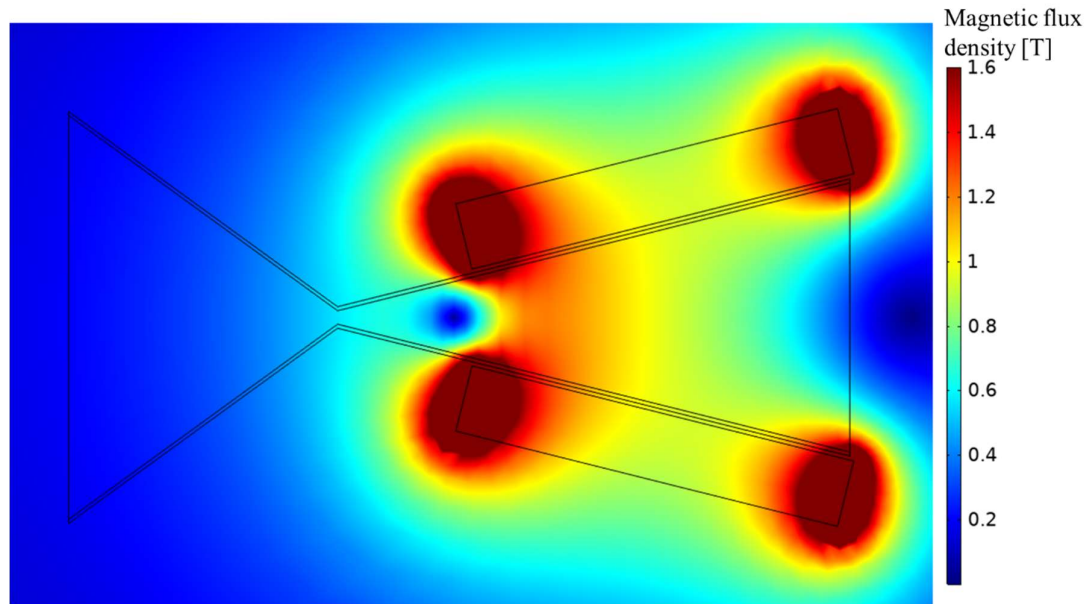


Figure 15

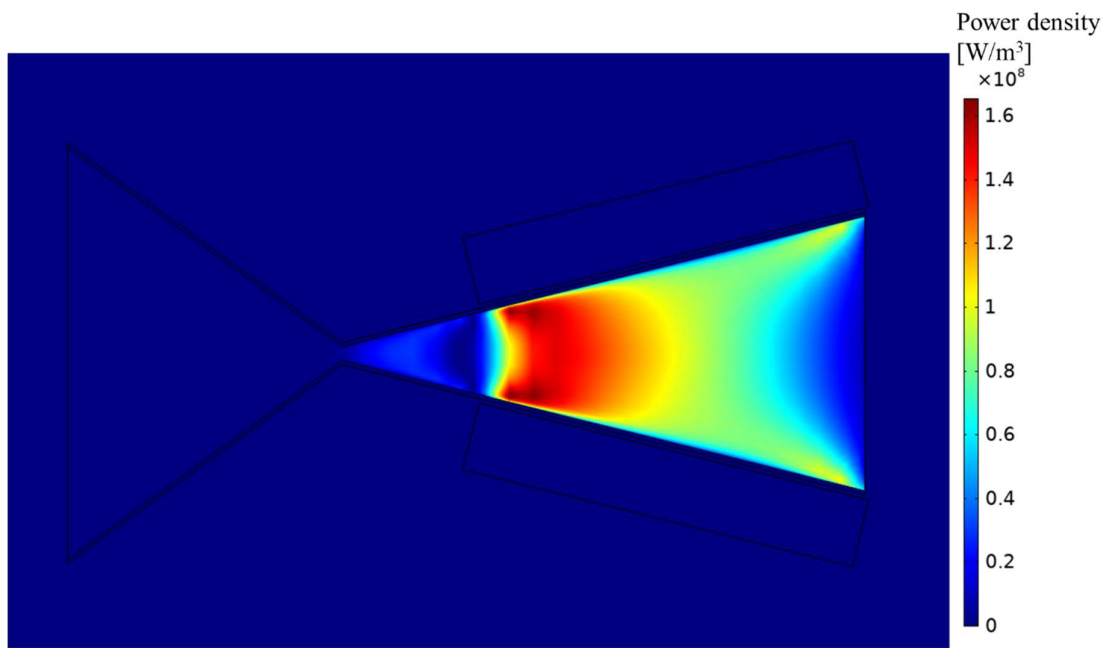


Figure 16